A New Two-Limit Control Strategy of a Levitating Motor

B SHAYAK
Sibley School of Mechanical and Aerospace Engineering,
Cornell University,
Ithaca – 14853, New York, USA
sb2344@cornell.edu , shayak.2015@iitkalumni.org
ORCID : 0000-0003-2502-2268

***Abstract*—In this work I propose a comparator-based control algorithm for a magnetically levitated motor, either induction or synchronous. The motor is two-channel, with a dipolar as well as a quadrupolar component. Each channel in the stator is supplied by a two-phase three-level or three-phase two-level voltage source inverter. The motor torque output is regulated via the dipolar channel, using the standard direct torque control protocols (DTC). Levitation and confinement of the rotor are achieved through the quadrupolar channel which is regulated by a novel two-limit control strategy, similar to DTC in philosophy and implementation. In the basic realization of this strategy, the measured parameters are the rotor displacements and the currents in the stator phases. A series of binary and ternary comparisons leads to a switching table which controls the states of the quadrupolar inverters. Simulation results show that this strategy leads to levitation and stabilization of the rotor. We then discuss a realization of the control strategy in which the explicit rotor position and velocity measurements are eliminated altogether and four laser beams fixed to the stator are used instead. The rotor bypasses or intercepts each beam depending on its displacement, and the states of the four beams are processed to generate the inverter switching table. Simulation results demonstrate the effectivity of this implementation, thus confirming the validity of the proposed control scheme.**

Keywords—Comparator control, Two-channel motor, Switching table, Voltage source inverter, Binary position sensor

I. INTRODUCTION

Direct torque control (DTC) of an induction motor was invented by Isao Takahashi and Toshihiko Noguchi in 1986 [1]. Two years later, a similar strategy called direct self control was proposed by Depenbrock [2]. DTC was the most significant landmark in the history of control of induction motors, representing a vast improvement over the existing standard of field-oriented control (FOC) [3], discussed in detail in Reference [4]. When DTC was later extended to permanent magnet synchronous motors [5,6] it again brought on a similar revolution on account of the simpler and more robust control architecture and apparatus. The superiority of DTC to the previously existing methods can also be understood clearly from Reference [7].

A control problem which is very relevant in today's age is that of magnetic levitation. Electromagnetic levitation of an object is rendered difficult by Earnshaw's theorem [8]. Magnetic bearings (levitators for rotating objects) have to overcome this theorem to be effective. There are two types of magnetic bearings in use – active and passive. In passive magnetic bearings [9-14] there is no control involved. These bearings use either superconducting materials or electromagnetic induction phenomena. The drawbacks with them are that superconductors are available only at cryogenic temperatures while designs involving eddy currents alone often do not generate a stiffness proportional to their size.

In active magnetic bearings, control is used to regulate the position of the rotor. A subset of active magnetic bearings is the bearingless (or self-bearing) motor which integrates rotation and levitation – this is the focus of the present Article. References [15,16] have proposed a novel design of a permanent magnet motor with controlled axial force. A similar design may be found in Reference [17]. References [18,19] on the other hand propose an architecture with radial control. The latter features a six-pole permanent magnet on the rotor and two sets of windings on the stator – a single phase six-pole winding and a separate three-phase four-pole one. A similar approach with different polarities has been demonstrated in Reference [20]. In References [21,22] the two separate windings have been integrated into one structure.

In all these prior works [15-22], we can see a large variety in the winding structure. The control algorithm used for the rotor position is however fundamentally the same. The position is measured and the stator currents required to generate a restoring force are calculated in the synchronously rotating d,q,o basis. These are then converted to the stator a,b,c basis and synthesized using an inverter. This strategy is very similar to FOC for the conventional induction motor. A typical block diagram of these strategies, taken from Reference [19], is reproduced in Fig. 1 (next page). The similarities with the block diagram for FOC [4] are noteworthy.

In this paper I will present the equivalent of DTC for a levitating motor. The stator consists of two concentric windings, one dipolar and one quadrupolar, and the rotor levitates inside the stator. Each winding is controlled by a three-phase two-level or two-phase three-level [23] voltage source inverter. The proposed control algorithm works entirely in the stator frame, thereby eliminating the need for online coordinate transformation. The processing of the displacements and forces is done through comparators and the selection of the voltage vector of each polarity is achieved via a switching table.

A knock-on effect of the new strategy is that an implementation is possible where the rotor position sensor is substituted by a set of laser beams which the rotor intercepts if it is displaced. The beams are received by detectors which turn ON if receiving the beam and OFF otherwise – the states of the detectors can be directly used to generate the inverter switching table, as will be explained presently. Thus, we can bypass the robustness and accuracy issues of position sensors

[24,25] while also circumventing the complexity of sensorless methods [26,27].

quadrature components of $\mathbf{i}_{r1}$, then the effective quadrupolar current of the rotor is $i_{r2d}^{\text{eff}}\cos 2\theta + i_{r2q}^{\text{eff}}\sin 2\theta$, where

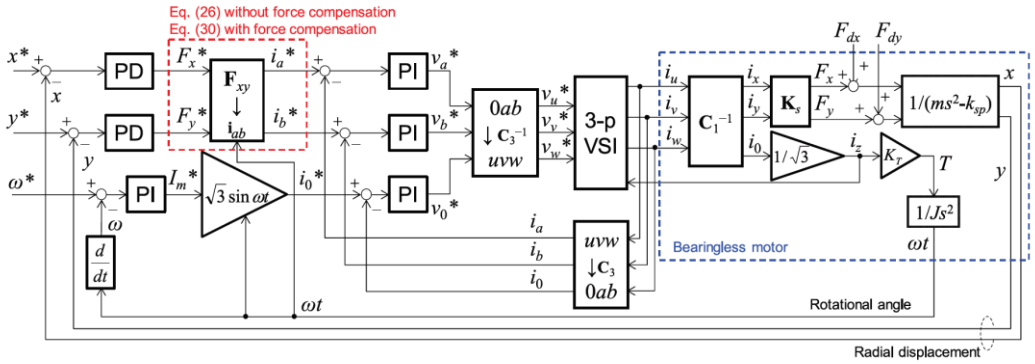

Figure 1 : *Block diagram of bearingless motor taken from Reference [19].*

II. Motor Dynamic Model and Solution

The dynamic model of the levitating motor is presented and solved in this Section. The induction motor is taken as an example since its dynamics is more involved. We consider a cylindrical, two-dimensional motor in cylindrical coordinates ρ,θ,z. Origin is taken to be at the centre of the stator. Cartesian coordinates x and y are also defined with respect to this origin, following conventional coordinate notations. The entire analysis will be carried out in stator frame coordinates, so the electrical d and q axes will also be defined in that frame. All currents flow along the z-axis (axis of symmetry) and are functions of θ. As already mentioned, the motor is a two-channel one with dipolar and quadrupolar channels. The dipolar current has the form $\cos\theta$ and $\sin\theta$ while the quadrupolar current has the form $\cos 2\theta$ and $\sin 2\theta$. We shall assume that only the stator can support a quadrupolar current – this component can be eliminated from the rotor by winding it such that the 2θ harmonic of its current is identically zero.

The evolution equations in space phasor form for the dipole channel are the usual [1,4]

$$\tau_{r1}\mathbf{i}_{r1}' + (1 - \mathrm{j}\tau_{r1}\omega)\mathbf{i}_{r1} + \delta_1(\mathbf{i}_{s1}' - \mathrm{j}\tau_{r1}\omega)\mathbf{i}_{s1} = 0\,, \qquad (1a)$$

$$\tau_{s1}\mathbf{i}_{s1}' + \mathbf{i}_{s1} + \delta_1\mathbf{i}_{r1}' = \mathbf{V}_1 / L_{s1}\ , \qquad (1b)$$

where $\mathbf{i}_{r1}$ denotes the dipolar rotor current phasor, $\mathbf{i}_{s1}$ denotes the dipolar stator current phasor, $\tau_{r1} = L_{r1}/R_{r1}$ is the rotor time constant, $\tau_{s1} = L_{s1}/R_{s1}$ is the stator time constant and δ_1 is a constant between zero and unity. Note that the subscripts r and s denote rotor and stator while subscripts 1 and 2 denote the dipolar and quadrupolar component. The motor torque is

$$\Gamma = C_1\left(i_{r1d}i_{s1q} - i_{s1d}i_{r1q}\right)\ , \qquad (2)$$

where C_1 is a proportionality constant.

The quadrupolar stator current satisfies an equation similar to (1b). Although the rotor does not carry a quadrupolar current, it turns out that the displacement of a purely dipolar rotor from the origin generates a non-zero quadrupole moment relative to the stator. If X and Y be the coordinates of the centre of the rotor relative to the origin, and i_{r1d} and i_{r1q} be the direct and

$$\mathbf{i}_{r2}^{\text{eff}} = (2/r)\mathbf{W}\mathbf{i}_{r1}\ , \qquad (3)$$

with $\mathbf{W}$ being the space phasor X+jY and r the rotor radius.

Using the previous relations, the quadrupolar stator current dynamics can be obtained in space phasor form as

$$\tau_{s2}\mathbf{i}_{s2}' + \mathbf{i}_{s2} = \frac{\mathbf{V}_2}{L_{s2}} - \frac{2\delta_2\tau_{s2}}{r}\left(\mathbf{W}\mathbf{i}_{r1}' + \dot{\mathbf{W}}\mathbf{i}_{r1}\right)\ , \qquad (4)$$

where the parameters have similar meanings as in (1). The overhead dot denotes time derivative for all variables other than i, where it creates confusion. The force on a dipolar rotor inside the stator's quadrupolar magnetic field is

$$\mathbf{F} = C_2\left[\left(i_{r1d}i_{s2d} + i_{r1q}i_{s2q}\right)\hat{\mathbf{x}} + \left(i_{r1d}i_{s2q} - i_{s2d}i_{r1q}\right)\hat{\mathbf{y}}\right]\ , \qquad (5)$$

where C_2 is some proportionality constant. The force is independent of the position of the rotor. It can be shown that the displacement of the rotor generates a correction to the torque over and above (2); this correction is

$$\Gamma_{\text{corr}} = C_1\left[\frac{X}{r}\left(i_{r1d}i_{s2q} - i_{s2d}i_{r1q}\right) + \frac{Y}{r}\left(i_{r1d}i_{s2d} + i_{r1q}i_{s2q}\right)\right]\ . \qquad (6)$$

The final equations in the model are the mechanical equations of the rotor :

$$m\ddot{X} + \gamma\dot{X} = F_x\ , \qquad (7a)$$

$$m\ddot{Y} + \gamma\dot{Y} = F_y - g\ , \qquad (7b)$$

where m is the rotor mass, γ is a damping constant and g is the acceleration due to gravity (we have taken it to be along $-y$-direction without loss of generality). Equations (1) to (7) make up the dynamic model of the bearingless motor.

We now solve these equations. In any DTC-style control algorithm, the inverter has an extremely small switching period T, during which time the applied voltage vector is a constant. T is taken to be considerably smaller than all other time-scales involved in the dynamics, because of which the solutions of the differential equations (1) to (7) may be Taylor expanded to first order in T before being reported, and

subsequently used. To solve the coupled system (1), the standard procedure is to make the resistanceless stator approximation i.e. to eliminate the term $\mathbf{i}_{s1}$ from the left hand side (LHS) of (1b). This done, we introduce the stator flux, $\boldsymbol{\psi}_{s1} = \mathbf{i}_{s1}+\delta_1\mathbf{i}_{r1}$, as a new variable. With this substitution, and setting $\tau_{r1} = 1$ and $L_{s1} = 1$, (1) and (2) read as

$$\dot{\boldsymbol{\psi}}_{s1} = \mathbf{V}_1 \ , \qquad (8a)$$

$$\mathbf{i}_{r1}' + \left(\lambda - \mathrm{j}\omega\right)\mathbf{i}_{r1} = \delta_1\left(-\dot{\boldsymbol{\psi}}_{s1} + \mathrm{j}\omega\boldsymbol{\psi}_{s1}\right) \ , \qquad (8b)$$

$$\Gamma = C_1\left(i_{r1d}\psi_{s1q} - \psi_{s1d}i_{r1q}\right) + \Gamma_{\mathrm{corr}} \ , \quad (8c)$$

where $\lambda = 1/(1-\delta_1^2)$. If $\boldsymbol{\psi}_0$ and $\mathbf{i}_{10}$ be the values of $\boldsymbol{\psi}_{s1}$ and $\mathbf{i}_{r1}$ at the start of a switching interval, and $\mathbf{V}_{10}$ be the dipolar voltage vector held during the interval, then the flux and current at the end of the interval are given by

$$\boldsymbol{\psi}_{+1}(T) = \boldsymbol{\psi}_0 + \mathbf{V}_{10}T \ , \qquad (9a)$$

$$\mathbf{i}_{r1}(T) = \mathbf{i}_{10} + T\left[\left(-\lambda + \mathrm{j}\omega\right)\mathbf{i}_{10} - \delta_1\mathbf{V}_{10} + \mathrm{j}\delta_1\omega\boldsymbol{\psi}_0\right] \ . \qquad (9b)$$

The change in torque during the interval, computed basis these expressions, agrees with what has been found in Reference [1] from a different solution process; it is not reproduced here.

The resistanceless stator approximation is also made on (4). If $\mathbf{V}_{20}$ be the quadrupolar voltage vector held during the switching interval, $\mathbf{i}_{20}$ the starting value of quadrupolar stator current, $\mathbf{W}_0$ the starting displacement phasor, $\dot{\mathbf{W}}_0$ the starting velocity phasor and $\mathbf{i}_{10}$' the time derivative of $\mathbf{i}_{r1}$ at the start of the interval, then $\mathbf{i}_{s2}$ at the end of the interval is given by

$$\mathbf{i}_{s2}(T) = \mathbf{i}_{20} + \frac{T}{\tau_{s2}}\left[\mathbf{V}_{20} - \frac{\delta_2}{r}\left(\mathbf{W}_0\mathbf{i}_{10}' + \dot{\mathbf{W}}_0\mathbf{i}_{10}\right)\right] \ . \qquad (10)$$

We now use (5) together with (9b) and (10) to calculate the change in F_x and F_y during the interval. When the vector $\mathbf{V}_{20}$ is zero, the expression on the right hand side (RHS) of (10) is difficult to evaluate and does not lend insight into the dynamics. When $\mathbf{V}_{20}$ is non-zero however, we can safely assume that it far exceeds the terms involving $\mathbf{W}/r$ since that is a small quantity. Making this assumption, we drop the second term in the coefficient of T in the RHS of (10). This now leads to the following :

$$F_x(T) = F_{x0} + T\begin{bmatrix} -\lambda\left(i_{10d}i_{20d} + i_{10q}i_{20q}\right) + \omega\left(i_{10d}i_{20q} - i_{20d}i_{10q}\right) - \\ \delta_1\left(i_{20d}V_{10d} + i_{20q}V_{10q}\right) + \delta_1\omega\left(\psi_{0d}i_{20q} - i_{20d}\psi_{0q}\right) + \\ 2\left(i_{10d}V_{20d} + i_{10q}V_{20q}\right) \end{bmatrix} . \quad (11)$$

Similarly,

$$F_y(T) = F_{y0} + T\begin{bmatrix} \lambda\left(i_{20d}i_{10q} - i_{10d}i_{20q}\right) - \omega\left(i_{10d}i_{10q} + i_{20d}i_{20q}\right) + \\ \delta_1\left(i_{20d}V_{10q} - V_{10d}i_{20q}\right) - \delta_1\omega\left(\psi_{0d}i_{20d} + \psi_{0q}i_{20q}\right) + \\ 2\left(i_{10d}V_{20q} - V_{20d}i_{10q}\right) \end{bmatrix} . \quad (12)$$

We shall interpret these expressions later. Finally, we solve the system (7). To linear order in T we have

$$X(T) = X_0 + v_{x0}T \ , \qquad (13a)$$

$$v_x(T) = v_{x0} + T\left(\frac{F_x - \gamma v_{x0}}{m}\right) \ , \qquad (13b)$$

$$y(T) = Y_0 + v_{y0}T \ , \qquad (13c)$$

$$v_y(T) = v_{y0} + T\left(\frac{F_y - \gamma v_{y0} - g}{m}\right) \ . \quad (13d)$$

Basis these expressions, we shall now devise the proposed control strategy.

III. The Control Algorithm

Here we use the mathematical results obtained above to formulate the control algorithm at the heart of the proposed magnetic levitator. We consider the two-phase stator construction with four non-trivial dipolar and quadrupolar voltage vectors available – these are along the positive and negative d and q axes. This enables a more compact representation of the algorithm with no conceptual differences from the three-phase case. The dipole channel is controlled via standard DTC as in Reference [1], with suitable modifications to account for a two-phase inverter. It is here that we exploit the absence of quadrupolar windings on the rotor – those would have generated an extra contribution to the torque, thus complicating the classical DTC algorithm unnecessarily.

The control of the displacements X and Y is of course the novelty of the present paper. For a robust control similar in style to DTC, we need everything to be based on comparisons alone – there can be no PID and similar controllers. We start from the list of quantities that need to be measured. The first quantity is the displacement (X,Y) of the centre of the rotor – an obvious requirement since we want to control it. It can be measured either by electrical, optical or acoustic sensor. Thereafter, we need the applied forces and the quadrantal position of $\mathbf{i}_{r1}$ (this requirement shall be explained presently). Since the rotor levitates, we would like to minimize measurements on it. Instead we measure the currents in all the stator phases, giving the phasor $\mathbf{i}_{s1}$; subtracting this from $\boldsymbol{\psi}_{s1}$ (whose value is known from the classical DTC algorithm) gives $\mathbf{i}_{r1}$. We note that measuring the rotor angular position in a conventional permanent magnet synchronous (or brushless dc) motor is very standard practice – since the angle sensors are not attached to the rotor, they are suitable for the levitating rotor also. The current measurement also gives us $\mathbf{i}_{s2}$, and we can then estimate the electromagnetic forces using (5).

We define tolerance displacements x_{tol} and y_{tol} (likely the same value but not necessarily so). Then, if $X > x_{\mathrm{tol}}$, we define the reference value of F_x to be a constant $-F_{\mathrm{set}}$. If $X < -x_{\mathrm{tol}}$, then we define the reference $F_{x,\mathrm{ref}}$ to be the constant $+F_{\mathrm{set}}$. If X lies in between the negative and positive tolerances, then $F_{x,\mathrm{ref}}$ is zero. In a similar manner, we define reference values for F_y.

Equation (5) tells us that the force arises from the interaction of $\mathbf{i}_{s2}$ and $\mathbf{i}_{r1}$. If we had a current source inverter at hand which could have synthesized arbitrary quadrupolar stator currents, and hence the reference forces, then we would have been done. However, that is not the case. A voltage source inverter can only cause a change in current and hence an increase or decrease in force. Hence, we now calculate the disparity

between the actual forces (estimated as described above) and the reference values. Let $F_{x,\mathrm{err}} = F_{x,\mathrm{ref}} - F_x$ and $F_{y,\mathrm{err}} = F_{y,\mathrm{ref}} - F_y$. Let the indicator variable s_x have the value 1 if $F_{x,\mathrm{err}}$ is positive i.e. $s_x = 1$ denotes a required increase in F_x, and similarly let $s_x = 2$ denote a required decrease in F_x. Analogously, let the indicator variable $s_y = 1$ and $s_y = 2$ denote required increases and decreases in F_y.

We now analyse (11,12). From the former equation we can see that the change in F_x during the switching interval contains five terms, among which the first four are predetermined by the state of the motor at the beginning of the interval. Only the last term depends on the quadrupolar voltage vector selected during the interval. This term can be expressed as the "dot product" of the phasors $\mathbf{i}_{10}$ and $\mathbf{V}_{20}$. If the voltage vector $\mathbf{V}_{20}$ is chosen such that this dot product is positive then there will be an increase in F_x, provided that the other terms are of the right size and sign (if they are not, then we will never be able to increase F_x and the setpoint F_{set} has been prescribed incorrectly relative to the motor parameters). Similarly, if $\mathbf{V}_{20}$ is chosen so that this dot product is negative, then there will be a decrease in F_x. Analogously, (12) shows that the increase and decrease in F_y is controlled by the entity $i_{10d}V_{20q} - V_{20d}i_{10q}$, which can be interpreted graphically as the "cross product" of the phasors $\mathbf{i}_{10}$ and $\mathbf{V}_{20}$.

This analysis implies that the choice of voltage vector depends on the quadrantal position of the vector $\mathbf{i}_{r1}$ relative to the d-q basis. If $\mathbf{i}_{r1}$ is in the first quadrant then an increase in both F_x and F_y is achieved by selecting $\mathbf{V}_{20}$ along the $+q$-axis, while an increase in F_x and decrease in F_y is achieved by selecting $\mathbf{V}_{20}$ along the $+d$-axis. Similarly, a decrease in F_x and an increase in F_y is achieved by selecting the vector along the $-d$-axis while a decrease in both F_x and F_y is achieved by selecting the vector along $-q$-axis. The required voltage vectors for other quadrantal positions of $\mathbf{i}_{r1}$ can be worked out in a similar manner. Note that quadrantal position gets replaced by sextant in a three-phase implementation with six available non-trivial voltage vectors.

The previous now suggests a three-dimensional switching table. Let s_4 be an indicator of the quadrantal position of the rotor current vector. Then, we construct a switching table $\mathbf{S}(s_4,s_x,s_y)$. Letting <1>, <2>, <3> and <4> denote the voltage vectors along the $+d$, $+q$, $-d$ and $-q$ axes, the switching table is as follows (a two-dimensional representation of the table is used to fit on the page) :

Table 1. The switching table for the selection of quadrupolar voltage vectors, depending on the indicator variables mentioned in the text.

$s_4 \setminus s_x, s_y$	1,1	1,2	2,1	2,2
1	<2>	<1>	<3>	<4>
2	<3>	<2>	<4>	<1>
3	<4>	<3>	<1>	<2>
4	<1>	<4>	<2>	<3>

We now summarize the algorithm presented here in the form of a code. I have written the code in Matlab since it is extremely similar to English prose and can be understood by all the readers.

```
01  if X>x_tol
02      F_xref = -F_set;
03  elseif X<-x_tol
04      F_xref = F_set;
05  else
06      F_xref = 0;
07  end

08  if F_x<F_xref
09      s_x = 1;
10  else
11      s_x = 2;
12  end

% Similar steps for y in place of x

13  if i_r1d>=0 && i_r1q>=0
14      s_4 = 1;
15  elseif i_r1d<0 && i_r1q>=0
16      s_4 = 2;
17  elseif i_r1d<0 && i_r1q<0
18      s_4 = 3;
19  else
20      s_4 = 4;
21  end
```

Thereafter the switching table is defined as follows :

```
22   ST2 = zeros(4,2,2); % initialization
23   ST2(1,1,1) = V22;

% Here V21 to V24 denote <1> to <4> of
Table 1. We define other entries of ST2
for the other values of s_4, s_x and s_y
following Table 1.
```

Finally, the selection of voltage vector given the indicators is one more line of code :

```
24 V20 = ST2(s_4,s_x,s_y);
```

A similar switching table for flux and torque of course controls the selection of the dipolar voltage vector. We have thus presented an algorithm for the selection of the inverter switching state in every interval basis the flux, torque and positional requirements.

IV. Additional Optional Control Blocks

The core of the control block is as given in Section III; now we consider two additional blocks which are optional but might be of considerable utility. The first block is relevant if there are significant periods when the rotor is quiescent automatically i.e. in the absence of control. The algorithm in its present form does not have an option of selecting zero quadrupolar voltage vector. Even if the rotor is automatically quiescent near the origin, then also the inverters keep switching back and forth. We can remedy this by defining a small threshold value F_{tol} and then replacing line 24 of Section III with the following algorithm :

```
01  F_xerr = F_x-F_xref;
02  F_yerr = F_y-F_yref;
03  F_err = sqrt(F_xerr^2+F_yerr^2);
04  if F_err<F_tol
```

```
05      V20 = 0;
06  else
07      V20 = ST2(s_4,s_x,s_y);
08  end
```

This block is optional because automatically quiescent rotor does not occur if say the control is being used to lift its weight against gravity.

The second optional block is required when there is very little intrinsic damping in the system i.e. γ is very low. Then, we can synthesize a damping force from the controller itself. For this we define two reference forces F_{set1} and F_{set2} instead of a single F_{set}, and define a (possibly zero) velocity threshold v_{tol}. Then we replace lines 01 to 07 of Section III with the following :

```
09  if X>x_tol
10      F_1 = -F_set1;
11  elseif X<-x_tol
12      F_1 = F_set1;
13  else
14      F_1 = 0;
15  end
```

```
16  if v_x>v_tol
17      F_2 = -F_set2;
18  elseif v_x<-v_tol
19      F_2 = F_set2;
20  else
21      F_2 = 0;
22  end

23  F_xref = F_1+F_2;
```

An identical code block for Y of course has to be constructed also. The block diagram of the proposed control scheme is shown in Fig. 2. The core block of Section III is shown in black and the optional blocks of this Section are shown in grey.

V. Simulation Results

We now present the simulation results of the control strategy. The parameter values I have chosen are as follows : $\tau_{r1} = \tau_{s1} = 1$, $\tau_{s2} = 1/2$, $\omega = 50$, $\delta_1 = 0.49$, $\delta_2 = 0.34$, $r = 0.2$, $m = 1$ and $g = 1$ (if gravity is present). The two-phase motor is considered here. Magnitude of the dipolar voltage vector is 400 while that of the quadrupolar vector is 300. The setpoints and tolerances are $|\boldsymbol{\psi}_{s1}|_{set} = 4$, $|\boldsymbol{\psi}_{s1}|_{tol} = 0.02$, $\Gamma_{set} = 1.2$, $\Gamma_{tol} = 0.01$,

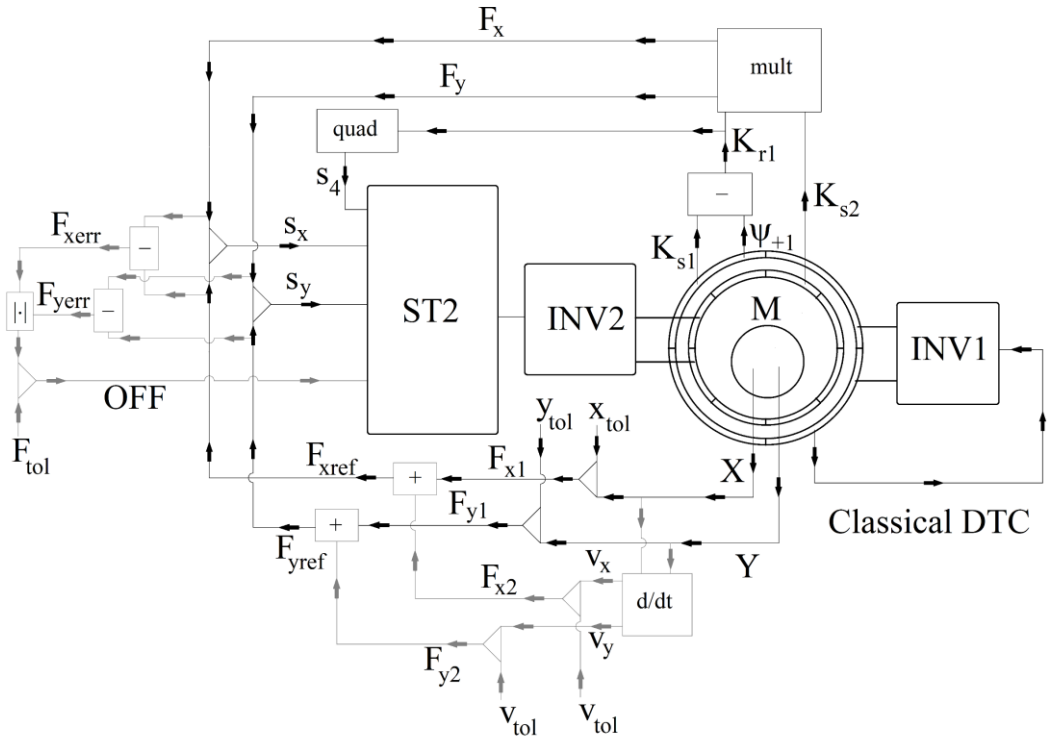

Figure 2 : *Placed here due to outsize. Block diagram for the proposed control strategy. M is the motor. INV1 is the inverter supplying the dipolar channel – it is controlled via standard DTC. INV2 is of course the quadrupolar one, whose actions are governed by the switching table ST2. A right-angled triangle denotes a comparator – the quantities to be compared enter along the hypotenuse while the output comes out of the vertex. The comparators are either binary (decide whether* a > b *or otherwise) or ternary (decide whether* a > b, a < –b *or otherwise). The details are given in the bulk text. The rectangles are miscellaneous calculators whose function is indicated by the symbol and explained in the text. Black elements form the core of the strategy (Section III) while grey elements are the optional blocks discussed in Section IV. It is instructive to compare this diagram with Fig. 1 and typical block diagrams of FOC and DTC of induction motors, for example from Reference [4].*

$x_{tol} = y_{tol} = 0.01$. The initial condition (IC) on dipolar flux is $\boldsymbol{\psi}_{s1}(0) = 4+j0$, the IC on rotor current is $\mathbf{i}_{r1}(0) = -0.036-j0.31$, the ICs on $\mathbf{i}_{s2}$ are zero, the ICs on displacement are $X(0) = Y(0) = 0.03$ and the ICs on velocity are zero. These all things remain invariant from run to run. Since several parameters have been set to unity, the units are not SI but arbitrary. For all simulations we have set the switching interval to be $T = 0.0003$ and run for ten lakh switching intervals.

Simulation is carried out in the following manner. We prescribe initial values of $\boldsymbol{\psi}_{s1}$, $\mathbf{i}_{r1}$, $\mathbf{i}_{s2}$, X, v_x, Y and v_y. These lead to initial values of the indicator variables for classical DTC as well as the new indicators s_4, s_x and s_y. These values act as initial conditions for the first switching interval. Then, we use the conventional switching table for DTC to select the dipolar voltage vector together with the new switching table ST2 to select the quadrupolar voltage vector. These voltage vectors are held during the switching interval. Given the voltage vector, we use (9) and (10) to update $\boldsymbol{\psi}_{s1}$, $\mathbf{i}_{r1}$ and $\mathbf{i}_{s2}$ to the end of the interval, and use (13) to update X, v_x, Y and v_y to the end of the interval. We recalculate the torque and forces at the end of the interval using (5) and (8c). We use the new X and Y to calculate the new references $F_{x,\text{ref}}$ and $F_{y,\text{ref}}$ and then compare them with the new forces F_x and F_y to update the indicator variables. We are now ready to select the voltage vectors for the next switching interval, and the process keeps on repeating, moving forward in time.

For the first run, the force setpoint is $F_{set} = 2$, the optional block for zero quadrupolar voltage is present but that for electrical damping is absent. We insert high mechanical damping $\gamma = 5$ since the voltage source inverter introduces delay into the system [28,29] and damping is necessary for stability. The time traces of X and Y are shown in Fig. 3.

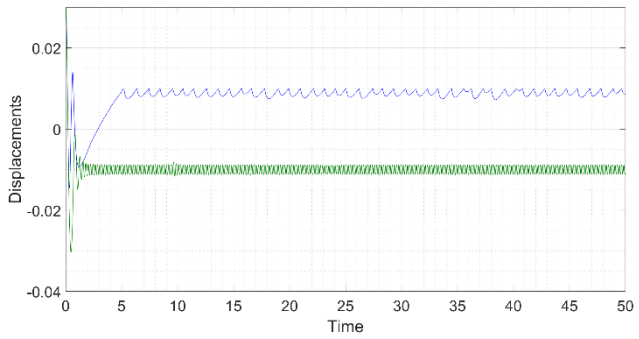

Figure 3 : *Rotor displacements vs. time in presence of gravity with mechanical damping.*

Here and in all subsequent plots we show X in blue and Y in green. We can see that X and Y are both immediately stabilized. The rotor position acquires a constant negative y-component on account of the gravity. A non-zero x-component also arises due to coupling inherent in the system. Although time trace of torque is not displayed, the effectivity of classical DTC has been verified in each case. We now insert the electrical damping block choosing $F_{set1} = 1.2$, $F_{set2} = 1.0$ and $v_{tol} = 0.01$. Mechanical damping γ is reduced to zero. The result, Fig. 4, is similar to Fig. 3.

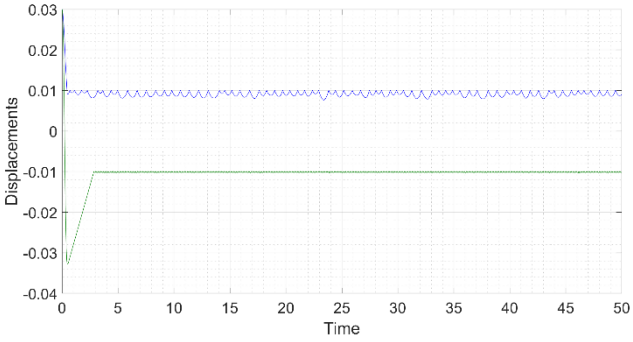

Figure 4 : *Same as Fig. 3 except with electrical damping synthesized through the controller.*

We see that the motor is completely stable even in this case.

VI. Beam-interception Implementation

The realization of the control algorithm in terms of binary position sensors is presented in this Section. Instead of the continuous position sensor as assumed heretofore, we have four laser beams fixed in the stator frame and running parallel to the motor axis. Let the beams be generated by torches at the top of the motor and received by photodetectors at the bottom. The distance between torch and receiver must be greater than the height of the rotor, which lies in the intervening space. The setup is shown in schematic form in Fig. 5.

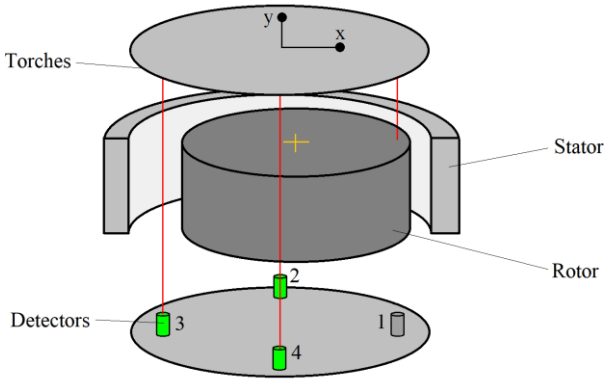

Figure 5 : *Beam-interception implementation of the control strategy. The red lines denote the laser beams, travelling from the torches to the detectors. They are fixed in stator frame. Each detector is ON (green) if it receives the beam and OFF (grey) if the beam is blocked. Beam 2 is directly behind beam 4 in this view. A positive* x*-displacement of the rotor has resulted in its blocking beam 1 and turning the corresponding detector OFF.*

The x-y coordinates of the four beams are $(r + x_{tol},0)$, $(0, r + y_{tol})$, $(-r - x_{tol},0)$ and $(0,-r - y_{tol})$ where r of course is the rotor radius. We label these beams as 1 to 4 respectively. Evidently, if the rotor is at its default position then all four beams bypass the rotor and travel smoothly from the torch to the detector. Displacements of the rotor cause it to intercept

the various beams. We program the controller as follows, letting d_1 to d_4 denote the state variables for detectors 1 to 4 and letting the value 1 denote ON and 2 OFF. Lines 1 to 7 of Section III become

```
01  if d1==2
02      F_1 = -F_set1;
03  elseif d3==2
04      F_1 = F_set1;
05  else
06      F_1 = 0;
07  end
```

An analogous logic of course holds for the *y*-direction. The optional damping block of Section IV can also be implemented in an approximate manner. We replace the continuous variables v_x and v_y with the variables p_x and p_y which are the signs of v_x and v_y. Thus, p_x and p_y can only have two values – positive or 1 and negative or 2. We realize that, for small displacements, a transition of detector 1 from OFF to ON indicates that the rotor is moving leftward while a transition of detector 3 from OFF to ON implies that the rotor is moving rightward. Hence we let these transition events define these two motion directions. In algorithmic terms, letting the integer the integer `ii` denote the current switching interval, so that `ii-1` obviously denotes the previous switching interval, we have

```
08  if d1(ii)==1 && d1(ii-1)==2
% detects a transition
09      p_x(ii) = 2;
10  elseif d3(ii)==1 && d3(ii-1)==2
11      p_x(ii) = 1;
12  else
13      p_x(ii) = p_x(ii-1);
14  end
```

The force reference commands are

```
15  if p_x==1
16      F_2 = -F_set2;
17  else
18      F_2 = F_set2;
19  end
```

Of course, similar algorithms hold true for the *y*-direction. It can be shown that for an oscillatory motion, this implementation of the damping block generates a positive damping for part of the cycle and a negative damping (driver) for the rest of the cycle. With properly chosen parameter values, the positive can outweigh the negative and stabilize the rotor. This is of course a jugaad solution constructed from the existing extremely simple apparatus – a different and more accurate method for measuring the sign of v_x and v_y, such as detecting the sign of induced emf in an eddy current sensor, can also be used.

For the simulations, we now replace the induction motor by a permanent magnet synchronous one. We assume that the rotor does not have pole saliency [4], so that the direct and quadrature axes inductances are equal and the space phasor model is applicable. Then, we can replace the dynamical variable $\mathbf{K}_{r1}$ with the algebraic equation $\mathbf{K}_{r1} = K_0\, e^{j\omega t}$ where K_0, the strength of the rotor current, is a constant. As usual, the dipolar channel controls the torque – DTC protocols for this are well established [5,6] and we ignore that part of the dynamics. The quadrupolar channel works just as before, except that we use the detector states to generate the reference forces, as described above.

For these simulation runs, we fix $K_{r0} = 4$ and $x_{tol} = y_{tol} = 0.01$. Gravity is present along the $-y$-axis as before. The condition for whether the rotor intercepts (respectively bypasses) each beam is that the beam must lie a distance less (respectively greater) than r away from the centre of the rotor. First we take mechanical damping $\gamma = 1$ with no electrical damping (Fig. 6) and then $\gamma = 0.01$ (which causes instability in the absence of electrical damping) with electrical damping based on the beam transitions (Fig. 7). For this, we define $F_{set1} = 2$ and $F_{set2} = 0.2$.

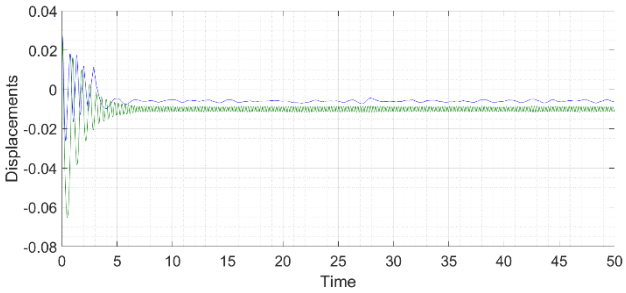

Figure 6 : *Rotor displacements vs. time in the beam-interception interpretation with mechanical damping.*

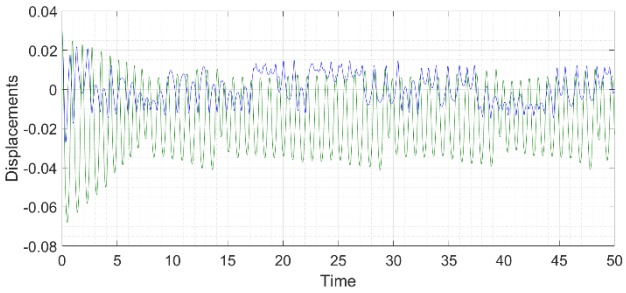

Figure 7 : *Same as Fig. 6 except with electrical damping synthesized by the controller.*

The effectivity of the strategy is clearly seen; mechanical damping provides a smoother response than the ad hoc electrical damper block.

VII. Conclusions

In this work we have seen a new two-limit control strategy of a magnetically levitated motor. Two 2-phase 3-level inverters or two 3-phase 2-level inverters are sufficient to achieve decoupled torque and position control of the rotor. The position sensor can be implemented in a binary form using laser beams which are blocked by the rotor's eccentricity.

Here we saw a two-dimensional motor model. We conjecture that a shaft mounted on two of the proposed bearingless motors, one at each end, can exhibit strong rotational stability even if the rotational angles are not measured. Rigorous demonstration of this is currently ongoing.

I hope that this control strategy can also be extended to maglev trains which are powered by linear induction and synchronous motors [30,31]. There too, a two-channel stator

winding with comparator-based control should enable a robust control architecture with decoupled and accurate control of the traction and the position.

Much more research has to be carried out to determine the optimal values of the various parameters, set points and tolerances which can lead to largest possible switching period, maximum use of zero voltage vectors, minimum inverter ratings and smallest possible displacement oscillations. The proposed drive also needs to be built in the laboratory. We leave these issues for future study.

REFERENCES

[1] I. Takahashi and T. Noguchi, "A New quick-response and high-efficiency control strategy of an induction motor," IEEE Transactions on Industry Applications 22 (5), 820-827 (1986)

[2] M. Depenbrock, "Direct self control of inverter fed induction machine," IEEE Transactions on Power Electronics 4 (3), 420-429 (1988)

[3] F. Blaschke, "The Principle of field orientation as applied to the new closed-loop transvector control systems for rotating field machines," Siemens Review 39 (2), 217-220 (1972)

[4] R. Krishnan, "*Electric Motor Drives – Modeling, Analysis and Control*," PHI Learning Private Limited, Nayi Dilli (2010)

[5] L. Zhong, M. F. Rahman, W. Y. Hu and K. W. Lim, "Analysis of direct torque control in permanent magnet synchronous motor drives," IEEE Transactions on Power Electronics 12 (3), 528-536 (1997)

[6] M. F. Rahman, L. Zhong and K. W. Lim, "A Direct torque controlled interior permanent magnet synchronous motor drive with field weakening," IEEE Transactions on Industry Applications 34 (6), 1246-1253 (1998)

[7] G. S. Buja and M. P. Kazmierkowski, "Direct torque control of PWM inverter-fed ac motors – a survey," IEEE Transactions on Industrial Electronics 51 (4), 744-757 (2004)

[8] DJ Griffiths, "*Introduction to Electrodynamics*," Third Edition, Pearson, Upper Saddle River, New Jersey, USA (2005)

[9] F. C. Moon and P. Z. Chang, "High speed rotation of magnets on high-Tc superconducting bearings," Applied Physics Letters 56 (4), 397-399 (1990)

[10] R. F. Post and D. D. Ryutov, "Ambient temperature passive magnetic bearings : theory and design equations," Preprint, UCRL-JC-129214 (1997)

[11] T. A. Lembke, "Design and analysis of a novel low loss homopolar electrodynamic bearing," Doctoral Thesis, Royal Institute of Technology, Stockholm, Sweden (2005)

[12] V. Kluyskens, B. Dehez and H. B. Ahmed, "Dynamical electromechanical model for magnetic bearings," IEEE Transactions on Magnetics 43 (7), 3287-3292 (2007)

[13] N. Amati, X. de Lepine and A. Tonoli, "Modeling of electrodynamic bearings," Journal of Vibration and Acoustics 130 (6), 061007 (2008)

[14] V. Kluyskens, C. Dumont and B. Dehez, "Description of an electrodynamic self-bearing permanent magnet machine," IEEE Transactions on Magnetics 53 (1), 8100409 (2017)

[15] W. Bauer and W. Amrhein, "Electrical design considerations for a bearingless axial force/ torque motor," IEEE Transactions on Industry Applications 50 (4), 2512-2522 (2014)

[16] W. Amrhein, W, Gruber, W. Brauer and W. Reisinger, "Magnetic levitation systems for cost-sensitive applications – some design aspects," IEEE Transactions on Industry Applications 52 (5), 3739-3752 (2016)

[17] H. Sugimoto, S. Tanaka, A. Chiba and J. Asama, "Principle of a novel single-drive bearingless motor with cylindrical radial gap," IEEE Transactions on Industry Applications 51 (5), 3696-3706 (2015)

[18] S. Zhang and F. L. Luo, "Direct control of radial displacement for bearingless permanent magnet type synchronous motors," IEEE Transactions on Industrial Electronics 56 (2), 542-552 (2009)

[19] J. Asama, T. Oi, T. Oiwa and A. Chiba, "Simple driving method for a 2-DOF controlled bearingless motor using one three-phase inverter," IEEE Transactions on Industry Applications 54 (5), 4365-4376 (2018)

[20] E. Severson, S. Gandikota and N. Mohan, "Practical implementation of dual-purpose no-voltage drives for bearingless motors," IEEE Transactions on Industry Applications 52 (2), 1509-1518 (2016)

[21] V. F. Victor, F. O. Quintaes, J. S. B. Lopes, L. D. S. Junior, A. S. Lock and A. O. Salazar, "Analysis and study of a bearingless ac motor type divided widing based on a conventional squirrel cage induction motor," IEEE Transactions on Magnetics 48 (11), 3571-3573 (2011)

[22] S. Kobayashi, M. Ooshima and M. Nasiruddin, "A Radial position control method of bearingless motor based on d-q axis current control," IEEE Transactions on Industry Applications 49 (4), 1827-1835 (2013)

[23] A. Nabae, I. Takahashi and H. Akagi, "A New neutral-point-clamped PWM inverter," IEEE Transactions on Industry Applications 17 (5), 518-523 (1981)

[24] R. L. Maresca, "A General method for designing low temperature-drift, high bandwidth, variable reluctance position sensors," IEEE Transactions on Magnetics 22 (2), 118-123 (1986)

[25] M. D. Noh, S. R. Cho, J. H. Kyung, S. K. Ro and J. K. Park, "Design and implementation of a fault-tolerant magnetic bearing system for a turbomolecular vacuum pump," IEEE/ASME Transactions on Mechatronics 10 (6), 626-631 (2005)

[26] A. Schammass, R. Herzog, P. Buehler and H. Bleuler, "New results for self-sensing active magnetic bearings using modulation approach," IEEE Transactions on Control Systems Technology 13 (4), 509-516 (2005)

[27] W. Gruber, M. Pichler, M. Rothboeck and W. Amarhein, "Self-sensing active magnetic bearing using 2-level PWM current ripple demodulation," Proceedings of the Seventh International Conference on Sensing Technology, 587-591 (2013)

[28] R. H. Rand, "Lecture Notes on Nonlinear Vibrations," available electronically at http://audiophile.tam.cornell.edu/randdocs/nlvibe52.pdf

[29] M. Davidow, B. Shayak and R. H. Rand, "Analysis of a remarkable singularity in a nonlinear DDE," Nonlinear Dynamics 90 (1), 317-323 (2017)

[30] I. Takahashi and Y. Ide, "Decoupling control of thrust and attractive forces of a linear induction motor using space vector control inverter," IEEE Transactions on Industry Applications 29 (1), 161-167 (1993)

[31] A. K. Rathore and S. N. Mahendra, "Direct secondary flux oriented control of linear induction motor drive," Proceedings of the 2006 IEEE International Conference on Industrial Technology, 1586-1590 (2006)